Monroe, C., and Beckermann, C., "Deformation During Casting of Steel: Mold and Material Properties," in Proceedings of the 61st SFSA Technical and Operating Conference, Paper No. 5.6, Steel Founders' Society of America, Chicago, IL, 2007.

Deformation during casting of steel: model and material properties

C. Monroe
C. Beckermann
Department of Mechanical and Industrial Engineering
The University of Iowa, Iowa City, IA 52242

Abstract

Dimensional differences between a final casting and its design are casting distortions. Distortion is created by the deformation occurring throughout solidification and further cooling during the casting process. Accurate prediction of casting distortion should be found through modeling the entire deformation. Modeling requires the knowledge of casting process conditions, material properties, mold restraint, and other factors. Solidification and further cooling simulation uses above process details to obtain temperatures. From the temperatures, the transient deformation and final distortions can be calculated. A generic mechanical property data set for low alloy steel is presented and the result of simulating deformation is compared to experimental measurements. This property data set was developed for a yield stress model that includes strain hardening and strain rate dependence.

Introduction

Distortion in any steel casting is costly. Added operations are required to finish the casting. Corrective changes to the design or the pattern tooling is done by trial and error. Process fluctuations can cause episodic appearances of unacceptable distortion during production. Prediction and a fundamental understanding of distortion are important when trying to control any part or process.

Casting simulation is used to predict solidification and cooling results. Understanding the process allows a casting designer or producer to make decisions that affect either the part or the rigging to optimize quality. Casting simulation tries to use physically realistic models without overtaxing the computer. The simulations need to give usable results in the shortest time possible. Simulating casting distortion has been done using (fast to simulate) simplified mechanical models that gave incorrect simulation results. This is true for hot tear modeling, where inadequate mushy zone modeling limited our ability to predict hot tears. Improving the mechanical models has been an incremental process. With each improvement, the predictions become a challenge to calculate in a fast and robust manner.

The latest progress in improvement is a yield stress model that incorporates isotropic strain hardening and strain rate dependent hardening. Temperature dependent material properties will be presented for this yield stress model. Then a casting example from a previous T&O illustrates the simulation process [1]. The new yield stress model is progress toward a more realistic model; but a final model with validation is not presented.

Method

The summary in Figure 1 shows an overview of the sequence of casting simulation modules. Casting simulation starts with a geometry defined by a CAD model of the casting, mold, gating, chills, risers, padding, etc. Geometric features and other variables are specified. Using the Preprocessor, this geometry is input into the casting simulation software where other information relating to the molten metal chemistry, pouring temperature, flow properties, thermodynamic properties, and mechanical properties must be set.

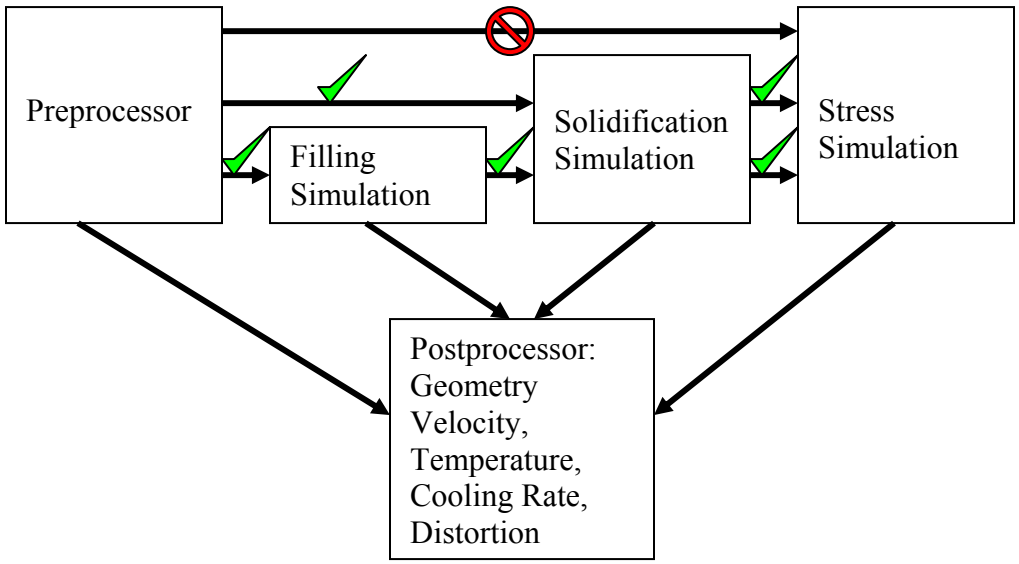

Figure 1. Flow diagram of the interrelationship of casting simulation modules.

After the CAD geometry is entered, the filling of the casting can be simulated. Once the filling event is modeled, the heat transfer during casting can be solved. The heat transfer calculation gives the temperature and porosity during solidification and further cooling. Porosity results are used to evaluate the casting soundness. Only after computing the temperatures and porosity can the deformation be evaluated. When deformation prediction is needed, an additional simulation is run. Temperature and porosity both drive deformation by casting shrinkage. In reality, deformation occurs at the same time as the temperatures are dropping and porosity is forming. It is usually accepted to calculate the deformation in a sequence and not as a codependent calculation. The validity of the distortion prediction is dependent on representative simulation results obtained for the temperature and porosity. Not only representative final results are needed, but the entire calculated history must be validated to predict the final casting shape and residual stresses.

Process measurements may verify the accuracy of the calculated values. For example, the temperature determined by a thermocouple is a check on the heat transfer calculation. The thermocouple data comparison ensures that the properties, simulation setup, and the calculation are all accurate. For deformation calculations, a “distortion probe” is necessary to check the simulation of strain. By checking the simulation of

deformation against experimental measurement, again the properties, setup, and calculation may all be validated. Once the simulation of the distortion is confirmed, then unwanted distortion of the casting may be reduced through design changes in the model. Using the deformation model to minimize unwanted distortion is the same as using thermal modeling of solidification to reduce shrinkage porosity. Validation of the deformation simulation motivates the casting experiments.

Material Mechanical Model

Mechanical properties vary with temperature, composition, cooling rate, etc. Obtaining usable mechanical properties up to the mushy zone temperatures is one challenge in the simulation of deformation. Three uni-axial tensile tests are shown schematically in Figure 2. Test A in the figure shows a test with a constant yield stress. Because no hardening occurs, the loading path ramps up in stress along the elastic slope initially. After reaching the yield stress, the loading continues yielding at a constant value. Test B in the figure shows the same loading path with the same initial yield stress but with strain hardening. Hardening acts to increase the yield stress with additional deformation. Test C illustrates a test, which has the same conditions as test B, at a higher strain rate. At high temperatures, the strain rate dependence is a viscous or creep problem. Creep describes materials that accumulate strain faster at increasing constant loads. The difference between test C and test B shows that while the strain hardening is similar, the strain rate dependence or creep requires a higher yield stress at a higher strain rate.

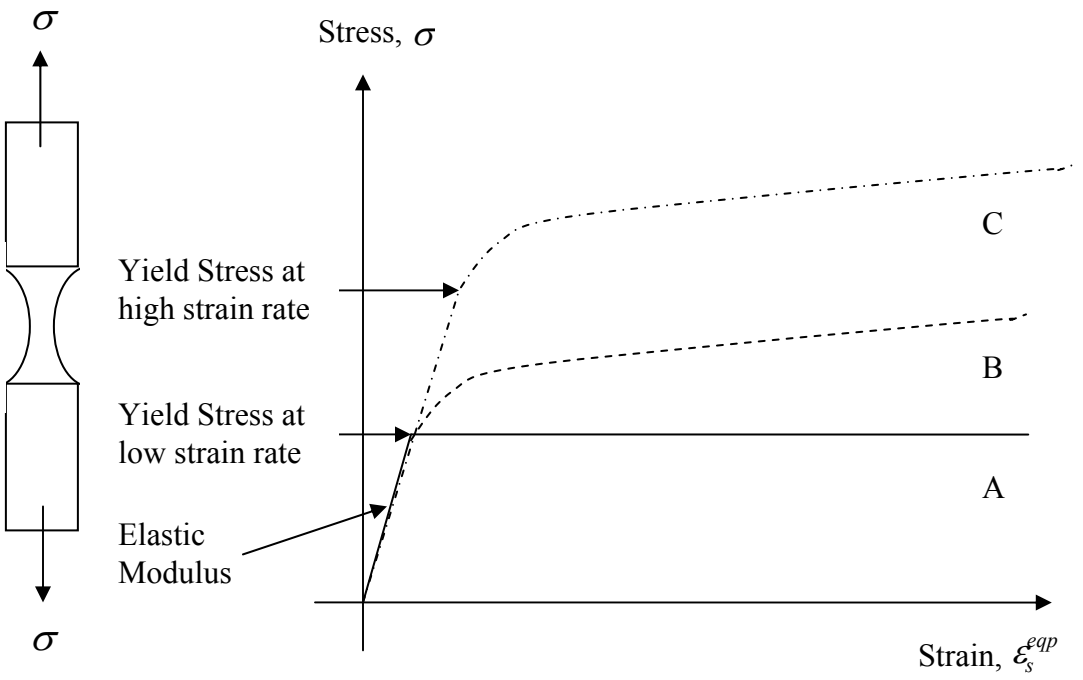

Figure 2. Schematic of a uni-axial stress-strain curve showing hardening and strain rate dependence.

The mechanical model used to describe the above process in uni-axial deformation begins with an assumption about the strains. This assumption is that the strain may be decomposed into three parts; the elastic, thermal, and inelastic (plastic or creep) parts. The equation is written as

$$\varepsilon = \varepsilon^{e} + \varepsilon^{th} + \varepsilon^{ie}.$$

The elastic strain behaves according to Hooke's law or

$$\sigma = C\varepsilon^{e},$$

where the elastic modulus is C and the stress is σ. The thermal strain is the integration of the change in density for the solid from the solidification temperature to the current temperature or

$$\varepsilon^{th} = \int_{T_{solidus}}^{T} -\frac{1}{\rho_s}\frac{\partial \rho_s}{\partial T}\,dT,$$

where the solid density is ρ_s, the temperature is T, and the solidus temperature is $T_{solidus}$. The stress state is calculated using the elastic modulus until the stress exceeds the yield stress. Whether the yield state is reached is calculated using the equation

$$F = \sigma - Y,$$

where the yield function is F and the yield stress is Y. This function is a scalar function that is always negative for elastic states, and is greater than zero when the inelastic strains are calculated. The inelastic strain is increased until the stress is reduced to match the yield stress. The inelastic strain required to keep the stress from exceeding the yield stress is found through the elastic equation above or

$$\sigma = C\left(\varepsilon - \varepsilon^{ie}\right).$$

A simple power law model may be used to describe the yield stress with hardening and creep. At lower temperatures, elastic properties are important. These properties are less determinative at high temperatures such as the temperatures in heat treatment or above. At high temperatures, yielding with hardening or creep dominates the deformation results. The following yield stress is used

$$Y\left(\varepsilon^{ie}, \dot{\varepsilon}^{ie}, T\right) = \sigma_o(T)\left(1 + \frac{\varepsilon^{ie}}{\varepsilon_o(T)}\right)^{n(T)}\left(1 + \frac{\dot{\varepsilon}^{ie}}{\dot{\varepsilon}_o(T)}\right)^{m(T)}$$

where the initial yield stress, $\sigma_o(T)$, the reference strain, $\varepsilon_o(T)$, the hardening exponent, $n(T)$, the reference strain rate, $\dot{\varepsilon}_o(T)$, and the strain rate exponent, $m(T)$, are all required to determine yielding. These values plus the elastic constants lead to a total of 7 temperature dependent properties that are needed to solve for deformation. This is not an unreasonable number of parameters. Many of these properties at room temperature are required to be determined for each heat by commercial specifications. Elastic modulus, initial yield stress, and hardening slope may all be obtained from a tensile specimen pulled at room temperature. The temperature dependent properties used for a generic low alloy steel will be presented. The model is similar to models proposed in any strength of materials book.

The above material mechanical model should be compared to previous yield definitions that are common in industry. The elastic modulus and Possion ratio, which are used to calculate the elastic strains, are the same as used historically. The yield stress model, however, is more elaborate. The additional features to account for hardening and creep effects may be turned off in this model by choosing the exponents that equal zero. In that case, the initial yield stress is the same as 0.2% yield stress that is obtained from room temperature tests. As a first approximation, the initial yield stress may always be chosen as the 0.2% yield stress. However as greater accuracy is required, especially at higher temperatures, the uni-axial tests should be fit at each temperature. The yield stress used when experimental curves are regressed may be much smaller than a 0.2% yield stress.

The material mechanical properties at room temperature up until 850 ^{o}C are obtained from the thermodynamic simulation software, Jmatpro 4.0 [2]. This software is supplemented at temperatures above 850 ^{o}C with experimental results of uni-axial tensile tests [3,4]. These two sources are joined piecewise at the common temperature to obtain consistent properties through the entire temperature range. The temperature dependent material inelastic properties above 850 ^{o}C are generated from completing a least-squares Levenberg-Marquardt minimization of simulated curves to the experimental points. A result comparing the experimental points to simulated uni-axial test is shown in Figure 3. The points represent the experimental measurement and the solid line is the calculated curve. Notice that the strain hardening is important in this test because the stress doubles from the small strain values to larger strains. The set of experiments consist of 102 uni-axial tensile tests which span 850 - 1450 ^{o}C, and 0.0 - 2.0 weight percent Carbon [wt%], 0.0 - 0.2 strain rate [in./in.]. Table 2 presents the linear fit of properties to the data as a function of temperature with the final coefficients.

Figures 4 and 5 show steel elastic properties, illustrating the property variation with temperature used in MAGMAsoft [5]. At low temperatures, the elastic modulus is high at about 205 GPa (29,700 ksi). As the temperature increases, the elastic modulus decreases to a low value at the highest temperature. As mentioned before, this variation is taken from Jmatpro 4.0 from room temperature to 850 degrees C. At higher temperatures, the property values are taken from the curve fit as given in published work [4]. These elastic properties are difficult to confirm. They may need additional revision based on experimental results relating the residual stresses to the high temperature deformation.

In Figure 5, the Poisson ratio increases in the solid from room temperature to the solidus temperature of the low alloy steel. Above the solidus temperature the ratio is not known. The variation of the Poisson ratio shown in the figure is multiplied by the solid fraction; note that the liquid, not the remaining solid, will be incompressible at the liquidus temperature (Poisson ratio equal 0.5).

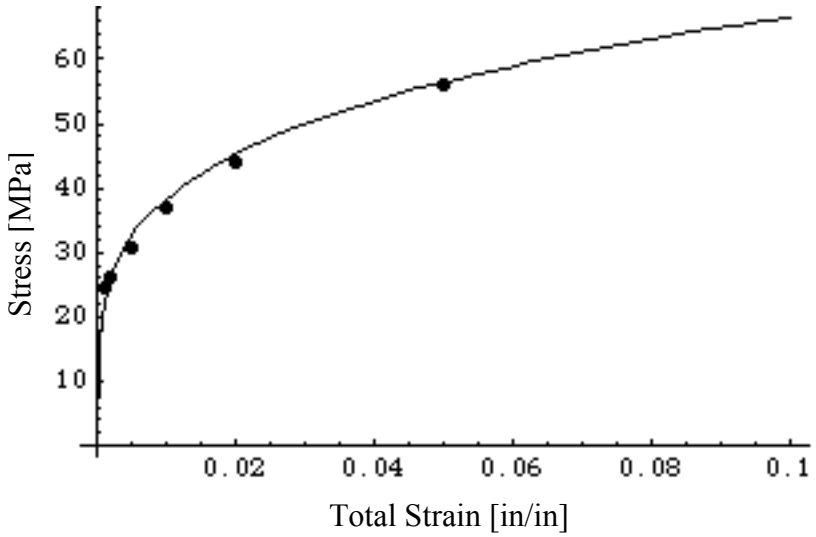

Figure 3. Typical result and curve fit for a single experiment.

Table 2. Equations for mechanical inelastic properties valid from 850 ^{o}C to 1400 ^{o}C

Property	Equation	Coefficient 1	Coefficient 2	Coefficient 3
Initial yield stress	$\sigma_o[\text{MPa}] = a_1 + a_2 * T[K]$	$a_1 = 1.93993$	$a_2 = -8.75426 * 10^{-4}$	
Hardening exponent	$n = b_1 + b_2 * T[K] + b_3 * C[wt\%]$	$b_1 = 0.362363$	$b_2 = -1.05482 * 10^{-4}$	$b_3 = -2.67962 * 10^{-2}$
Reference strain	$\varepsilon_o = \frac{\sigma_o n}{E}$			
Creep exponent	$m = c_1 + c_2 * T[K] + c_3 * C[wt\%]$	$c_1 = -0.042048$	$c_2 = -1.38125 * 10^{-4}$	$c_3 = -7.32437 * 10^{-3}$
Reference strain rate	$\dot{\varepsilon}_o[\text{s}^{-1}] = (d_1 + d_2 * T[K]) * \exp\left(\frac{Q}{T[K]}\right)$	$d_1 = 6438.2$	$d_2 = 11638.3$	$Q = 36000$

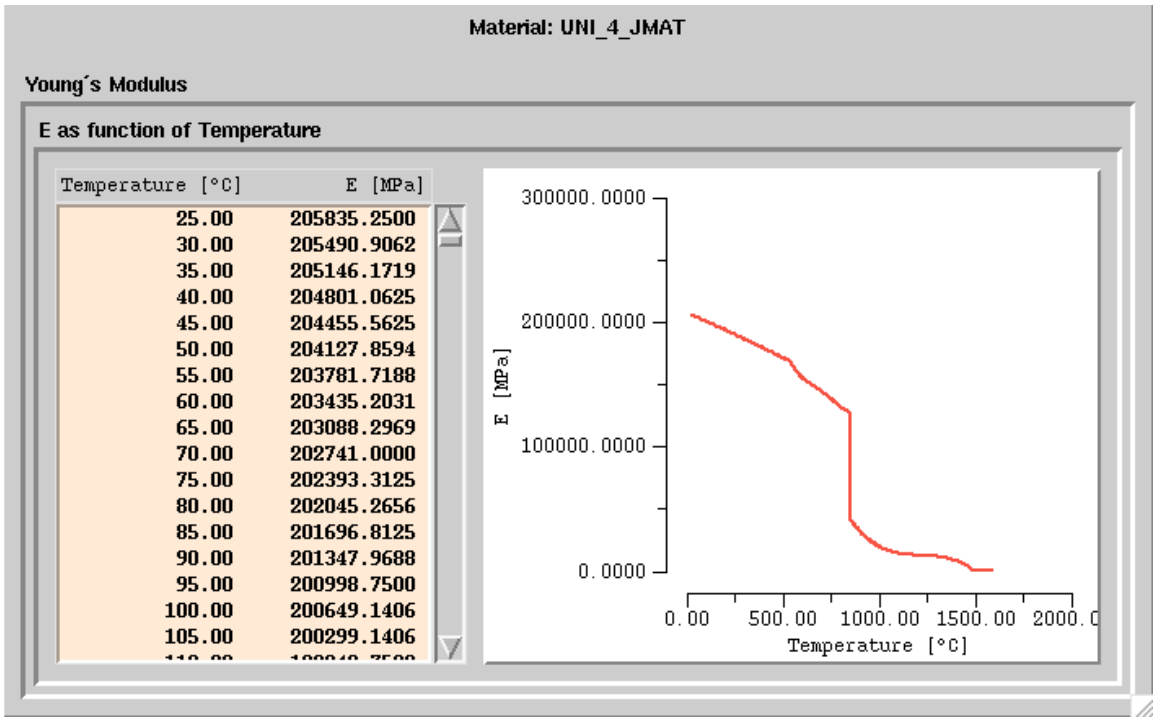

Figure 4. Low alloy steel elastic modulus curve variation against temperature. Note that at 850 ^{o}C the elastic modulus is joined piecewise from Jmatpro and previous published data [2,4].

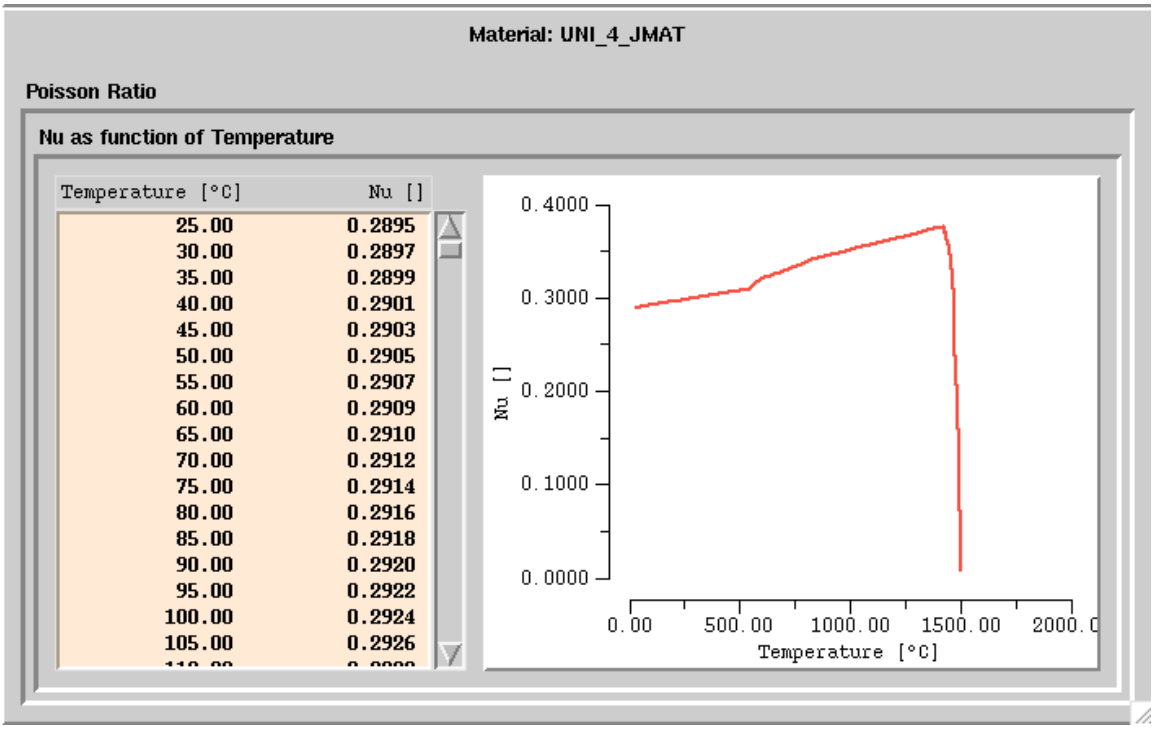

Figure 5. Low alloy steel Poisson ratio curve variation against temperature.

Figures 6 and 7 show plastic steel properties. In Figure 6, the yield stress at room temperature is determined by a tensile test. This value taken from Jmatpro is about 250 MPa (36 ksi). At high temperatures, the value of the initial yield stress decreases. The yield stress above 850 ^{o}C is not the same as the 0.2% offset yield stress. The initial yield stress was found by analyzing the experimental data published in reference 3. In Figure 7, the inverse of hardening exponent is shown. In MAGMAsoft, the inverse hardening exponent is used rather than the exponent shown in the above equation for the yield stress. The inverse hardening exponent increases with temperature. The reference strain is not shown in a figure because it is calculated from the other parameters. The formula for the reference strain is shown in Table 2. These plastic parameters may be used without the rate dependent part by setting the rate dependent exponent to zero.

Figures 8 and 9 show the rate dependent or creep properties. Strain from creep causes heat treatment distortion and relaxation of the residual stresses. In casting, creep is not as significant due to the low strain rates from smaller cooling rates as compared to heat treatment. The strain rate exponent increases with temperature as shown in Figure 8. Below 850 ^{o}C, the strain rate exponent is set to zero. Figure 9 shows the reference strain rate, which assumes some activation energy and coefficient. The reference strain rate decreases according to an Arrhenius law to a constant minimum value at low temperatures. These are summarized in Table 2.

In the next section, the rate dependence is not considered. Instead the creep exponent is set to zero at all temperatures. All the other properties are used as shown. MAGMAsoft currently allows no rate dependence. Therefore, current capability is demonstrated pending further model improvement. The following casting example shows the temperature and distortion results for comparison but not for validation purposes.

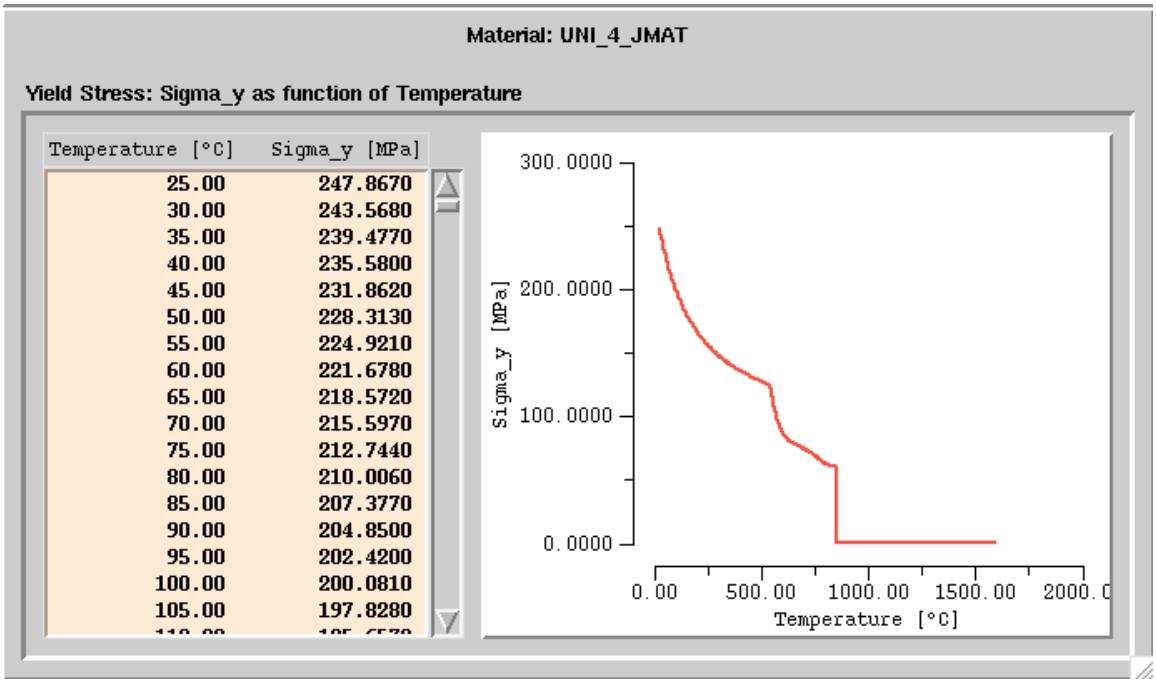

Figure 6. Low alloy steel initial yield stress (not a 0.2% offset yield) curve variation against temperature.

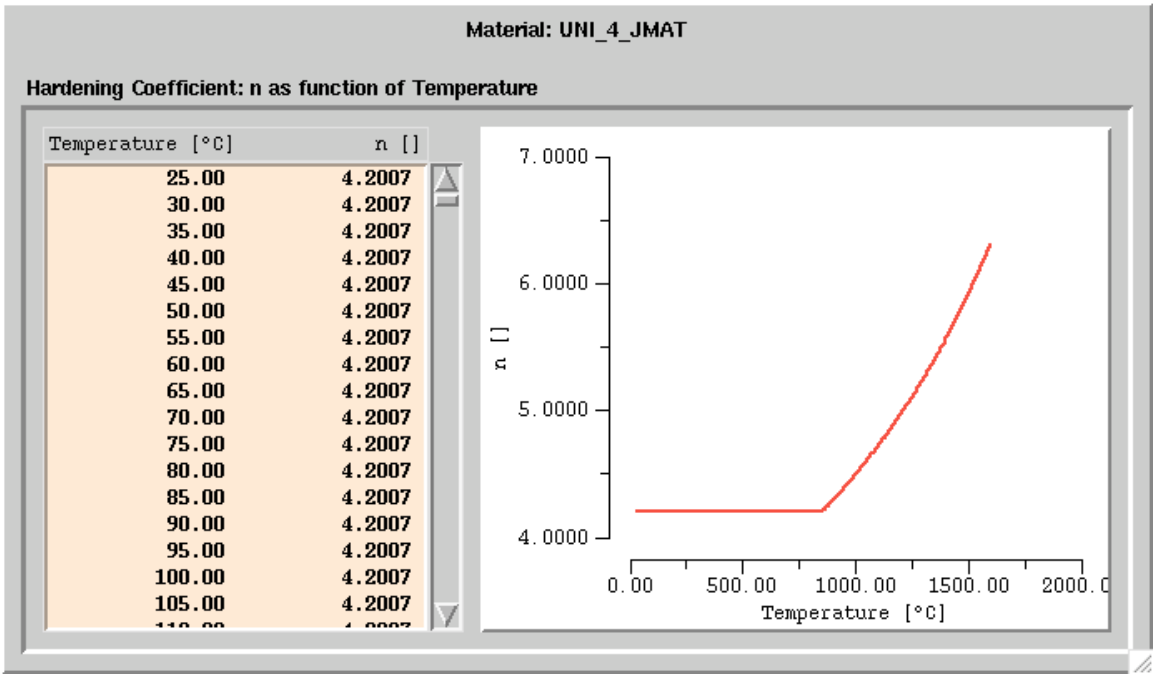

Figure 7. Low alloy steel inverse hardening exponent curve variation against temperature.

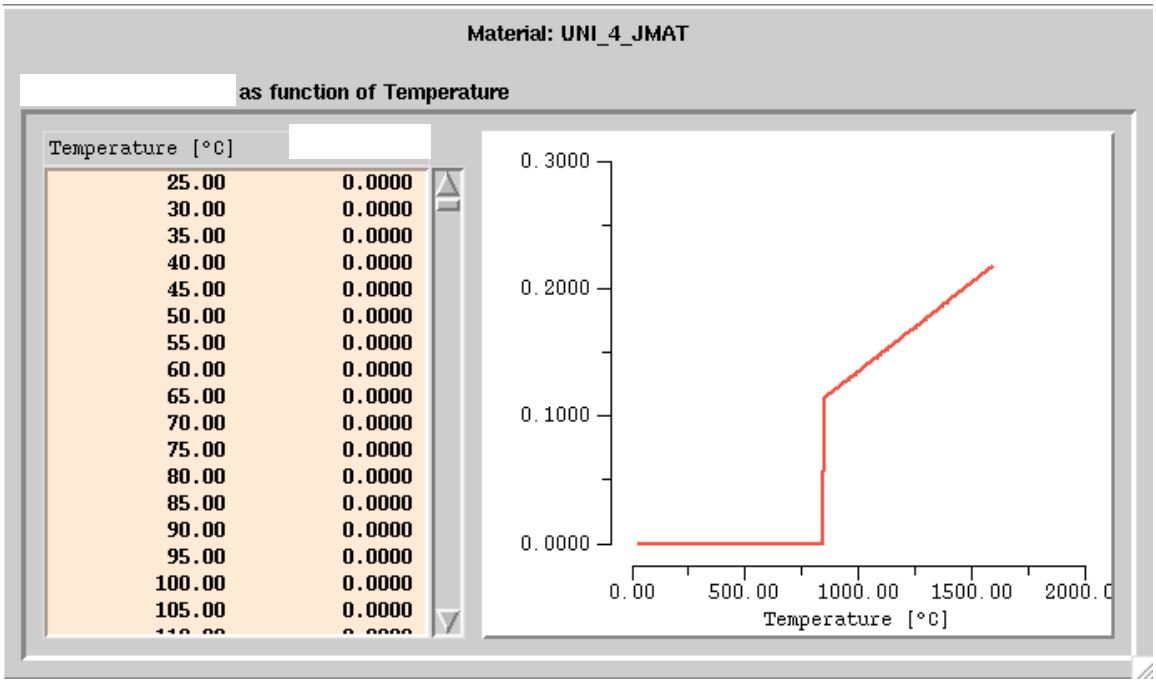

Figure 8. Low alloy steel strain rate exponent curve variation against temperature.

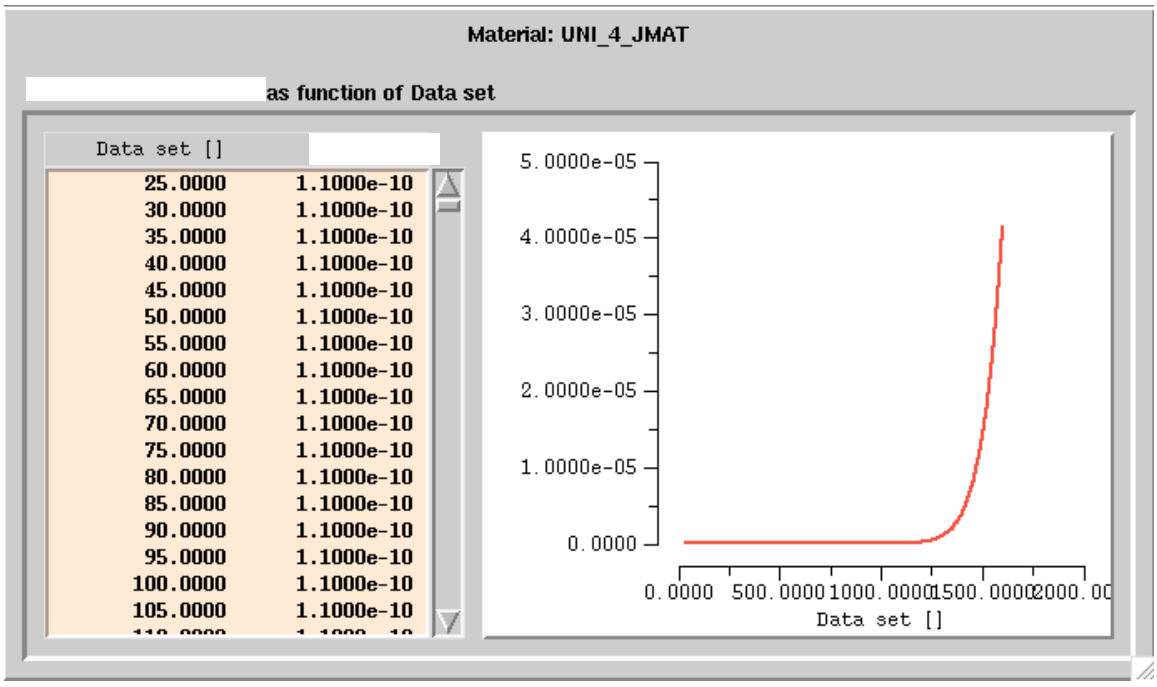

Figure 9. Low alloy steel reference strain rate curve variation against temperature.

Casting Example

The casting example shown demonstrates a comparison using a "distortion probe" which is a tool for validating the transient deformation simulation. The casting geometry and setup with results were presented at the last T&O [1]. The example was a result where no hot tears are expected because there was little restraint on the hot spot section. The setup of this casting is shown in Figure 10. The mold is shown in a light grey, the casting is in red, and the gating is in solid grey. The dimensions of the long bar section are 1" by 1" by 36". This ASTM A216 Grade WCB carbon steel casting was poured at the University of Northern Iowa. This casting was expected to shrink to the unrestrained shrinkage factor, patternmaker's shrink, across every dimension. In two locations dimensional data was measured during the casting process.

The experimental setup is shown in the schematic in Figure 11. Labels D2 and D4 indicate the locations of the dimensional probes. There are no bolts or force measurements in this casting trial. The probes are quartz rods that are installed in the mold running from outside the mold to the casting surface. On the end of the quartz rod that is outside the mold, a linear voltage displacement transducer (LVDT) records the location of the casting surface. In addition to the dimensional probes, a thermocouple is placed in the hot spot to record the temperature for validation of the temperature simulation.

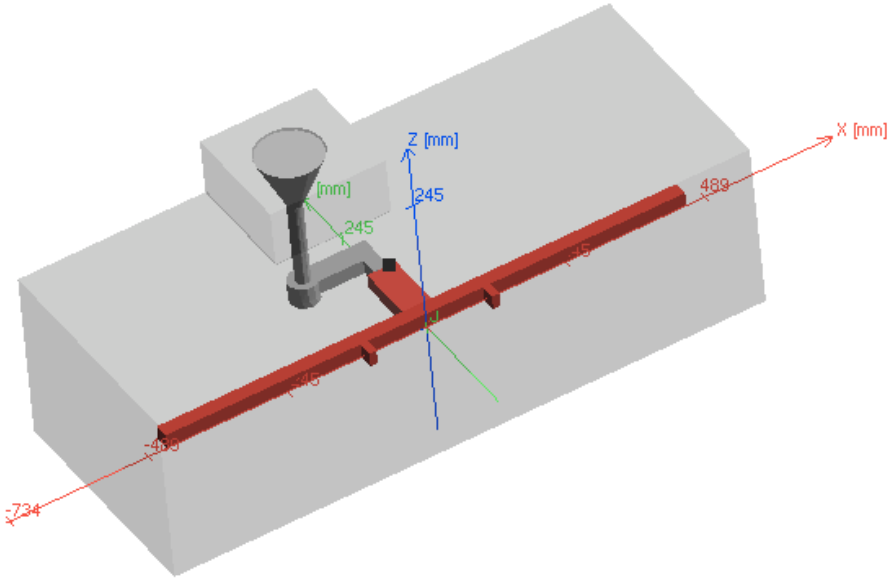

Figure 10. The isometric view of the casting setup in MAGMAsoft. The casting is in red and the gating is in solid grey. The mold is shown transparent in light grey.

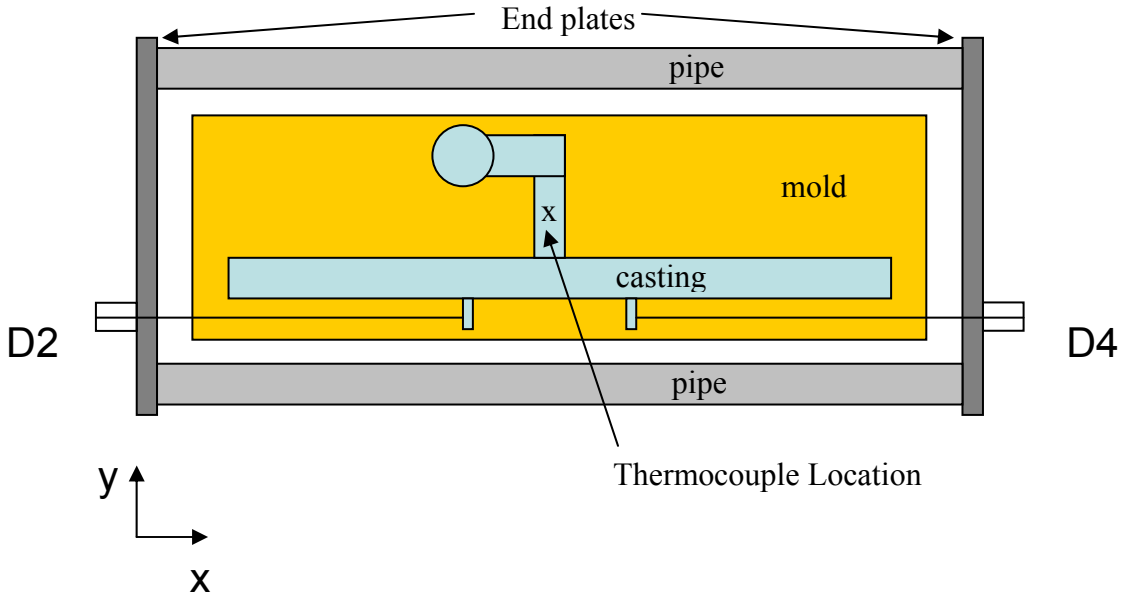

Figure 11. Schematic showing casting setup and probe locations.

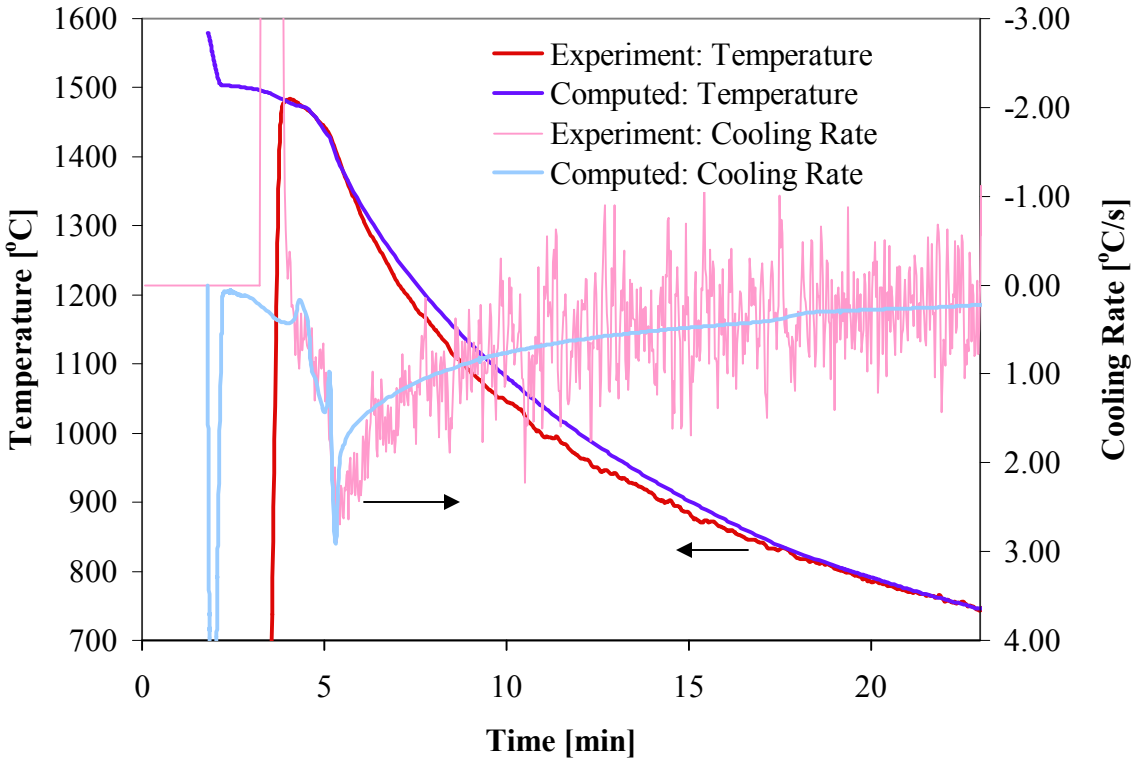

Figure 12. Comparison of the experimental thermocouple data to the simulation temperatures over the first 25 minutes of cooling.

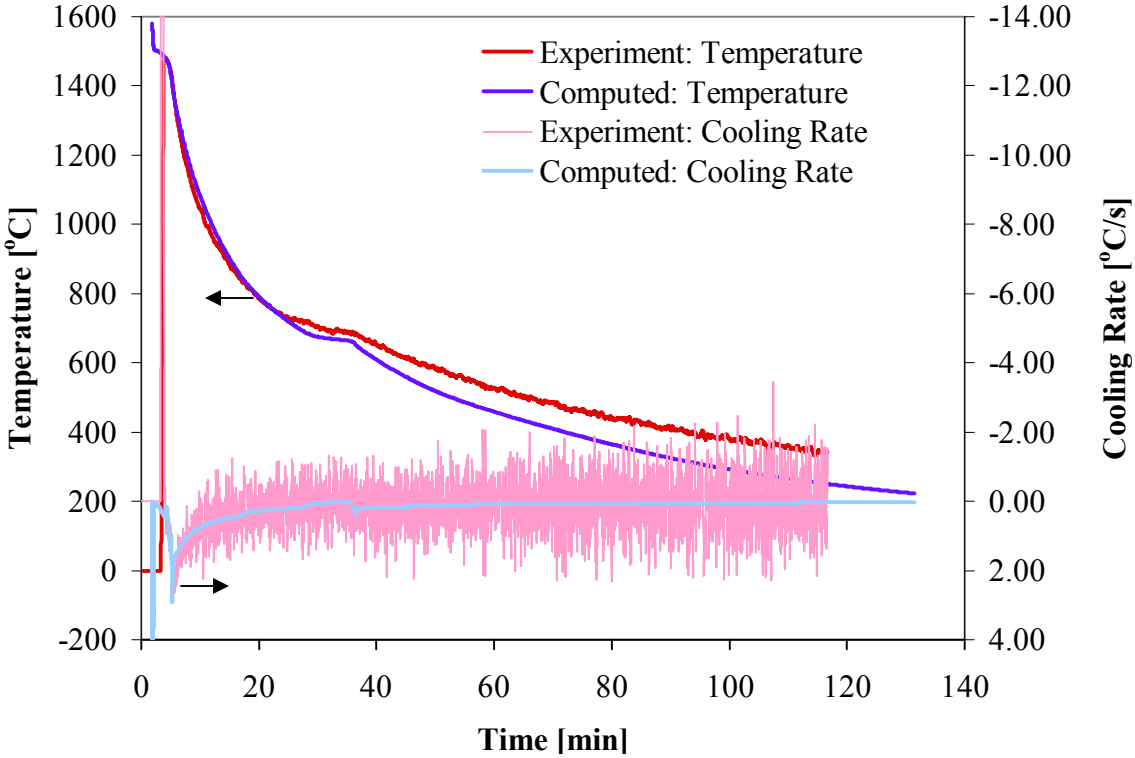

Figure 13. Comparison of the experimental thermocouple data to the simulation temperatures over the entire cooling.

Using the geometry in Figure 10, the filling event and heat transfer are calculated. Figures 12 and 13 show the temperature agreement of the thermocouple and the simulated temperature. This must agree not only in the solidification temperature interval but also down to the final temperature. This is needed for accurate prediction of the entire deformation behavior. The above temperature and cooling rate agreement is sufficient for the purposes of this comparison, however does not illustrate perfect agreement. The temperature arrests at both the solidus and again at the solid state transformation at around 30 minutes and about 650 ^{o}C in the experiment.

A new MAGMAstress algorithm is used for the simulation of the deformation. New features of this simulation include a finite element solution and new material models. One new feature is the contact model. The old contact model in MAGMAsoft joins two materials together as a single final material with fused contact. Where the material would always be in contact, such as around cores, this works well. In general, casting surfaces will pull away from the mold, core, or other interacting body. The new MAGMAstress algorithm has implemented a contact model with air gap formation and contraction around a core.

The temperature in the casting at ~1.5 hrs is shown in Figure 14. The undeformed geometry is shown at the top and a deformed casting geometry is shown on bottom. A magnification factor of 10 has been applied to the deformation. The simulation of deformation does not include the mold. This result indicates that the casting without the mold will uniformly contract. The space between the tabs off the long bar can be considered a gauge length. Figure 14 shows that the change from the original gauge length to the current gauge length, which changes in time, is the gauge displacement. Also it can be seen that the gauge displacement is a negative number indicating that the gauge length is contracting. In Figure 15, the simulation of distortion is shown with the mold contact included. Notice that an air gap does form in unrestrained dimensions. In restrained dimensions, the contraction of gauge length is restricted by the mold. If the mold is similar in strength to the metal this resistance may be expected to be important.

The change in the gauge length over time is shown in Figure 16. The experimental curve shows the change in position for the probe locations D2 and D4. The change in gauge length with time can be compared to similar points in a simulation. This transient data shows that the gauge closes over the entire experiment. At the Austenite to Ferrite decomposition temperature, an arrest in the closing behavior is seen at about 20 minutes into the experiment. At the phase transformation, the solid expands. After expansion, the solid continues to shrink during further cooling. In the case of no mold restriction, the gauge length shrinks to the expected patternmaker's shrink, ~2.4%, or 4.9 mm in this case. The mold was modeled using a single temperature independent elastic modulus. No thermal expansion or plasticity was included in modeling the mold deformation. In this small parametric study, the mold stiffness was varied from 1500 MPa to 3000 MPa. The final value of elastic modulus was set at 2250 MPa. For reference, the elastic modulus of silica is about 98000 MPa, and for unbonded sand about 150 MPa. Increasing the mold stiffness acts to restrict the shrinkage of the gauge length. This mold effect is most significant early in cooling, ~20min. After the casting cools to a low temperature with greater strength, the mold stiffness no longer prevents casting movement. A reasonable model for mold deformation and suitable properties must be included to predict casting distortion and hot tearing tendency.

The above simulations illustrate prediction of casting transient deformation and final distortion. The accumulated yielding, movement, stresses, etc. are all included from the pouring to final shakeout. All of the filling temperatures and heat transfer temperatures must be known to predict the deformation. In addition, the temperature dependent properties for the metal and the mold must be known. Although the simulation result appears reasonable with the appropriate choice of mold stiffness, it is not known whether this value for the elastic modulus of the mold is correct or even if modeling the mold as elastic is correct. Further validation is being studied to continue improving the models, properties, and simulations. The goal is to have a prediction that may be used as an engineering tool to improve casting design and optimize for more robust casting process with minimum defects.

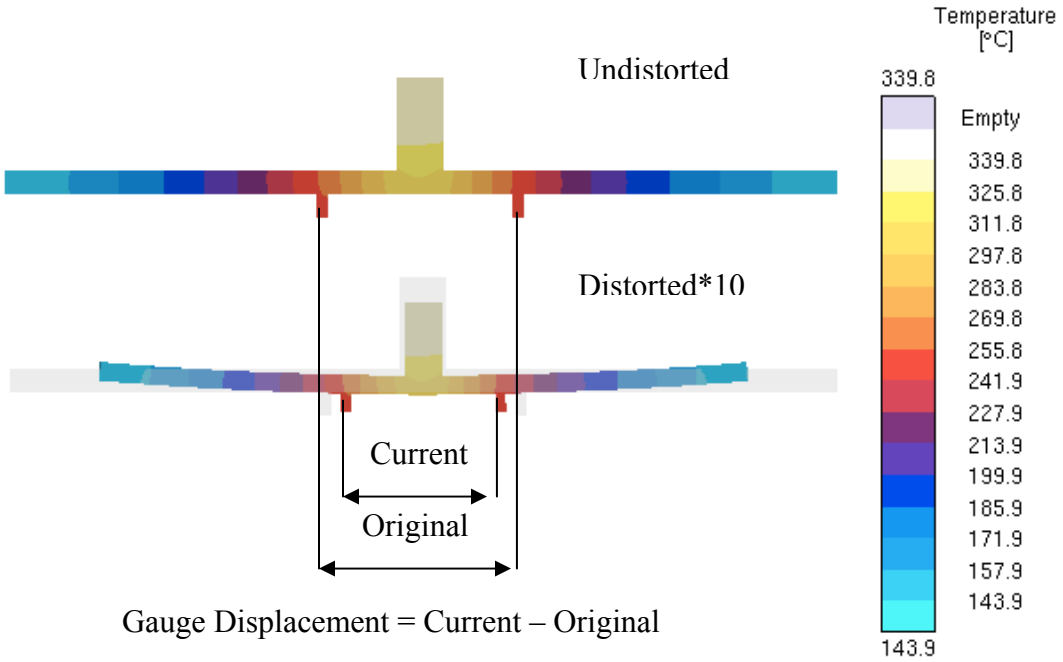

Figure 14. Temperatures at ~1.5 hours into the simulation without the mold of the experiment. The temperatures are shown on a distorted casting geometry that has been magnified by a factor of 10.

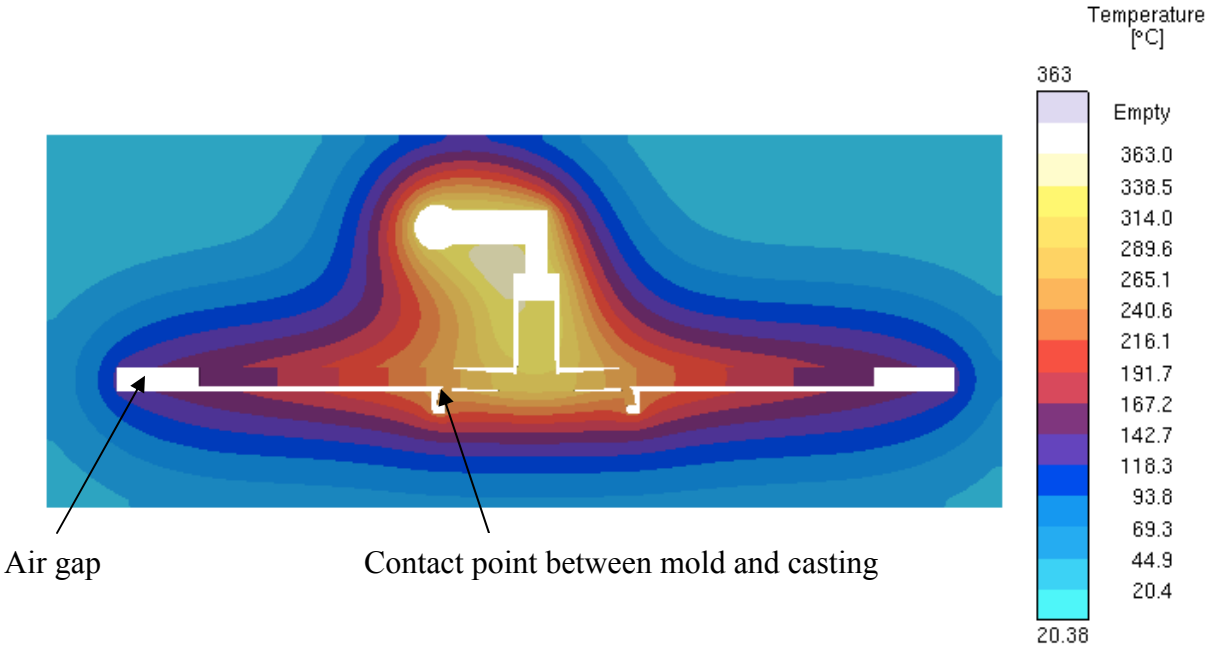

Figure 15. Temperatures at ~1.5 hours into the simulation with the mold of the experiment. The temperatures are shown on a distorted casting and mold geometry that has been magnified by a factor of 10. The air gap around the casting is shown in white.

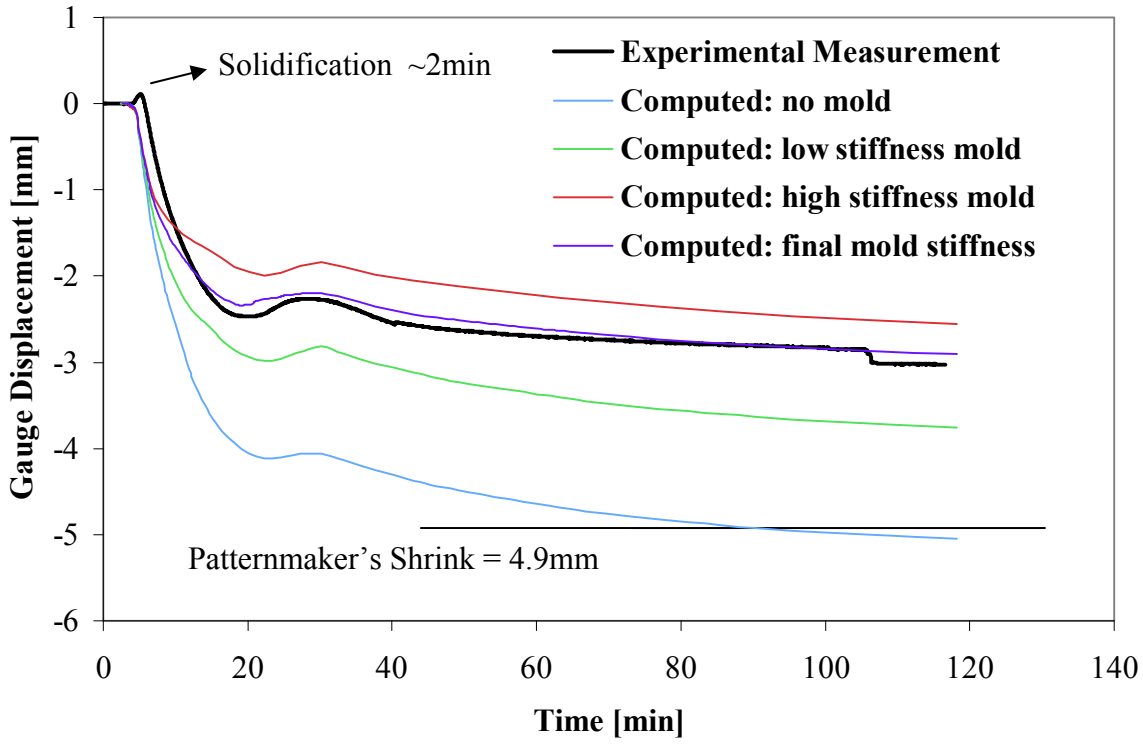

Figure 16. Graph showing the gauge displacement closing either to patternmakers shrink for the simulation with no mold or to the experimental value with the proper choice of mold stiffness.

Discussion

Temperature dependent material mechanical properties for low alloy steel used for modeling are shown. These properties are from high temperature experimental data and Jmatpro. MAGMAsoft is shown to give reasonable distortion prediction for a casting with mold restraint. The entire transient deformation process from pouring to shakeout is measured experimentally and compared to simulation. Results would be useful for reducing distortion and to predict the final properties.

Acknowledgements

This work was prepared with the support of the U.S. department of Energy (DOE) Award No. DE-FC36-04GO14230. However, any opinions, findings, conclusions, or recommendations expressed herein are those of the authors, and do not necessarily reflect the views of the DOE. The authors wish to that the Steel Founder's Society of America, especially Malcolm Blair and Raymond Monroe for their assistance in this work.

References

1. C. Monroe and C. Beckermann, "Simulation of Hot Tearing and Distortion during Casting of Steel: Comparison with Experiments," Steel Founders Society of America, T&O, December 2006.
2. *Jmatpro 4.0*, Sente Software Ltd., Surrey Tech. Center, 40 Occam Road, Guildford GU2-7YG, United-Kingdom.
3. P.J. Wray, "The effect of carbon content on the plastic flow of plain carbon steels at elevated temperature," *Metallurgical Transactions A*, 13A, 1982.
4. P. Kozlowski, J. Azzi, and B.G. Thomas, "Simple constitutive equations for steel at high temperature," *Metallurgical and Materials Transactions A*, 23A, 1992.
5. *MAGMAsoft*, MAGMA GmbH, Krackerstrasse 11, 52072 Aachen, Germany.